THE RICE INSTITUTE

POLARIZATION OF THE BREMSSTRAHLUNG FROM THE DECAY OF LITHIUM-8

by

JOHN GLEASON CRAMER, JR.

A THESIS

SUBMITTED TO THE FACULTY

IN PARTIAL FULFILLMENT OF THE

REQUIREMENTS FOR THE DEGREE OF

MASTER OF ARTS

Houston, Texas
May 1959

G. M. Glass
4/28/59

TABLE OF CONTENTS

I. Introduction

The research described herein is concerned principally with the detection of circular polarization in the bremsstrahlung produced when the longitudinally polarized electrons from the decay of Li^8 are slowed in lead. These electrons are polarized as a consequence of the non-conservation of parity in weak interactions.[1] The degree of left circular polarization of the bremsstrahlung has been shown to be a nearly linear function of the photon energy with a maximum polarization of about one when the photon energy is equal to the electron's energy.[2, 3] This theoretical result has been confirmed by a number of investigators for low energy beta decay (3 mev.).[4, 5, 6, 7] The end-point energy of Li^8 is about 14 mev. and while there is no reason to suspect a deviation from the theory at high energies, the total absence of any evidence provides ample reason for investigation.

Electrons which are transversely polarized can also give rise to circularly polarized bremsstrahlung, but the polarization varies radically with energy and should be easily distinguishable from the effect produced by longitudinally polarized electrons.[3]

To detect the circular polarization of the bremsstrahlung, advantage was taken of the dependence of the Compton cross section of magnetized iron on polarization. It has been shown[8] that if the iron is magnetized in the direction of propagation of the photons, then the ratio of the transmission of left to right circularly polarized photons

is: $T_{lcp}/T_{rcp} = e^{2NLv\sigma_1}$ where N is the number of atoms/cm^3, L is axial length of the magnet, v is the number of polarized (valence) electrons per atom, and σ_1 is the polarization dependent part of the Compton cross section. Since σ_1 is negative for photon energies above 0.63 mev., the transmission is greater for right than for left circular polarization. This effect provides a means of detecting a particular polarization by measuring the change in transmission with field direction.

However, before the polarization measurement could be undertaken, it was necessary to establish the energy spectrum of the external bremsstrahlung. This spectrum is also of interest in its own right, since there is some evidence[7] that it may deviate from theoretical predictions.

With the foregoing in mind, the investigations proceedes as follows. The external bremsstrahlung was made by converting the betas from Li^8 into bremsstrahlung with a thin lead radiator. The spectrum of the bremsstrahlung was then measured with a scintillation counter. To study polarization the bremsstrahlung was passed through magnetized iron before detection in the counter. The difference in transmission with the magnetization parallel and anti-parallel to the direction of propagation gave a measure of the polarization.

Some preliminary efforts have also been made to study the spectrum and polarization of inner bremsstrahlung. There are experimental difficulties, to be discussed later, which obscure the measure-

ment, but there are good reasons for making the investigation. Until quite recently, it was supposed that the type of interaction predominant in beta decay was the scalar-tensor type, although possibility of the axial vector-vector interaction was not excluded. Now the results of several experiments,[9,10,11,12] indicate that the interaction is of the axial vector-vector type. A measurement of the polarization of inner bremsstrahlung would provide additional evidence as to the type of interaction involved, since the direction of polarization depends entirely on the type of interaction and is in opposite directions for scalar-tensor and axial vector-vector interactions.[13]

II. Experimental Methods

The Li^8 needed in the measurements is most conveniently made with the $Li^7(d,p)Li^8$ reaction. The Li^7 targets were made by evaporating natural lithium onto an aluminum backing between 5 and 12 mils thick. The lithium layer was made sufficiently thick (about 25 mg/cm^2) to stop the deuteron beam at 2 mev. in order to maximize the Li^8 yield and also to prevent deuteron reactions in the aluminum target backing. The target holder assembly is a long tube of aluminum with an o-ring at the end which seals the target to the holder when the vacuum is applied, thus also supporting the target. It is constructed so that there is a minimum of material in the immediate vicinity of the target. This and the thinness of the target backing reduced the amount of extraneous external bremsstrahlung produced in the measurements to a small value.

The thickness of the lead converter must also be chosen carefully, since the yield and spectral distribution of the bremsstrahlung depends quite strongly on the converter thickness. This dependence is shown in Fig. 1. Notice that the low energy yield peaks at a greater thickness than the high energy yield. This is due to the thick target bremsstrahlung effect, and due to calculational difficulties discussed in Appendix III it is better to avoid this effect as much as possible. Therefore, we use a lead converter 0.032" thick, which is in effect a compromise between maximum yield and minimum thick target effects. To stop the betas not stopped in the target and converter with a minimum of bremsstrahlung the target assembly was surrounded by a paraffin sphere 2-1/2" in radius which could be slipped over the target holder. Since the bremsstrahlung are essentially in the same direction as the incident electrons, no special collimator was necessary.

Li^8 decays by negative beta emission with a half-life of 0.83 sec. The reactions accompanying the production of Li^8 products are such that a very high background is present while the beam is on. In view of this a pulsed beam technique was used. The deuteron beam was allowed to bombard the target for a period of time comparable to the half-life of Li^8 and then interrupted for an equivalent period, during which measurements were made. Thus the difficulties caused by the reaction product background were reduced.

To accomplish this interruption of the beam, it was passed between a pair of parallel plates[14] which deflected the beam when a voltage was applied to them. This voltage was produced by an 8 KV power supply[14] and applied to the plates by a specially designed pulse

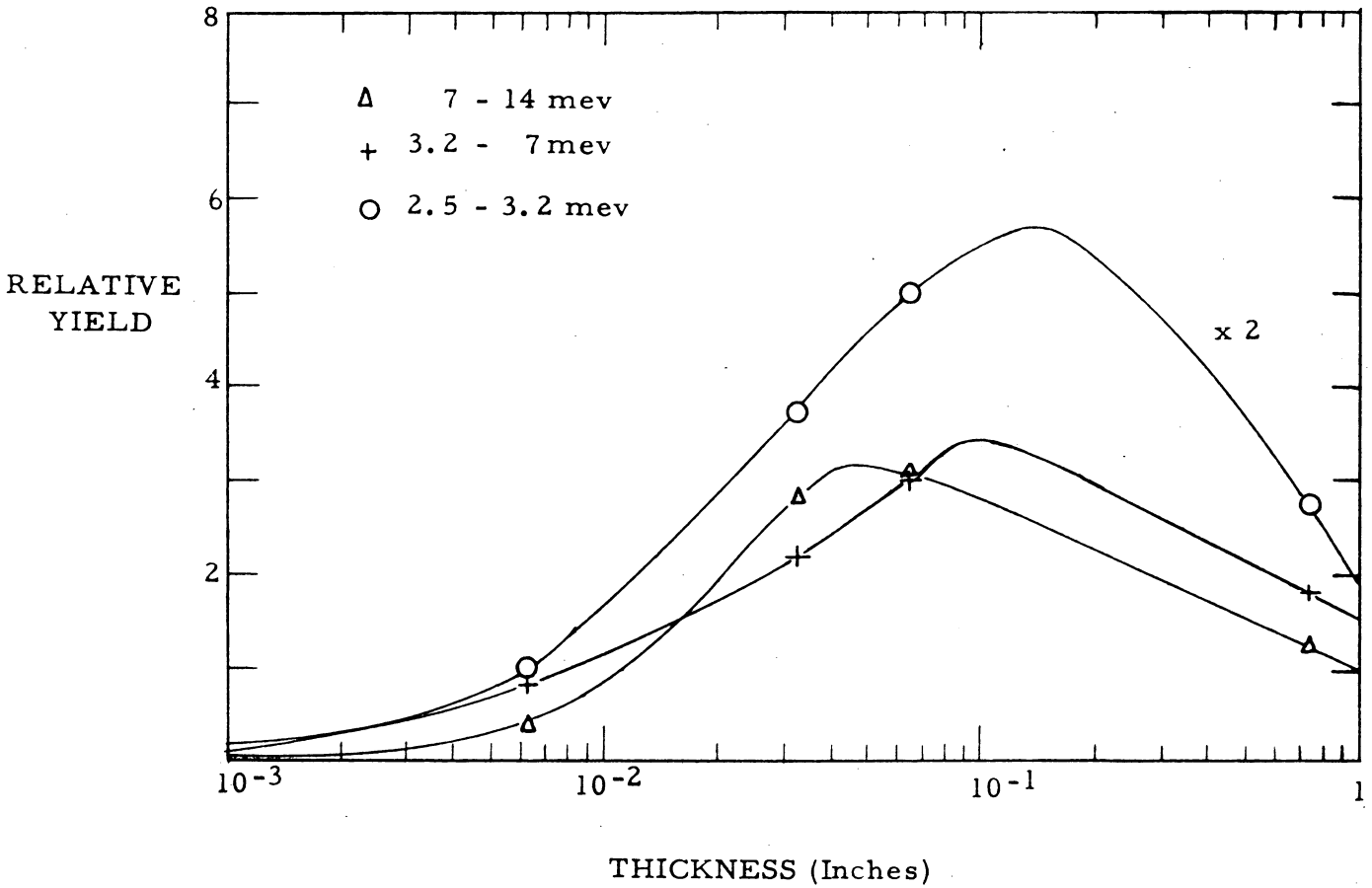

Figure 1 YIELD OF BREMSSTRAHLUNG VS CONVERTER THICKNESS

control unit.[14] This unit contains a square wave generator and a 6BK4 high voltage regulator tube. The control unit is shown in Fig. 2. The square wave generator serves two purposes. First, it applies a square wave switching signal to the regulator tube. Second, it produces another signal which is nested inside the signal mentioned above. This signal controls the operation of the scintillation counter. This nesting feature assures that the beam is completely off before the counter comes on and the counter is completely off before the beam comes on. The unit is devised so that the voltage is switched between a high value and a low value which is considerably above ground potential. Thus the beam is always deflected to some extent but the degree of deflection is switched. The system is aligned so that if the deflection is too small as well as too large the beam is stopped by tantalum slits. This prevents any uncharged beam, which would not be deflected, from striking the target while the beam is supposed to be off the target. Fig. 3 shows this alignment and the path of the beam under each of these circumstances.

The preamplifier used in conjunction with this system is shown in Fig. 4. It is of standard design except for the circuit involving the focusing electrode. The focusing electrode is used to gate the photomultiplier, a technique first suggested by Fornelli and Nalvano[15] who found that this was the most effective way of gating the tube without introducing sizeable switching transients and gain shifts. Notice that the 6AU6 switch tube circuit plugs into the preamp proper, and

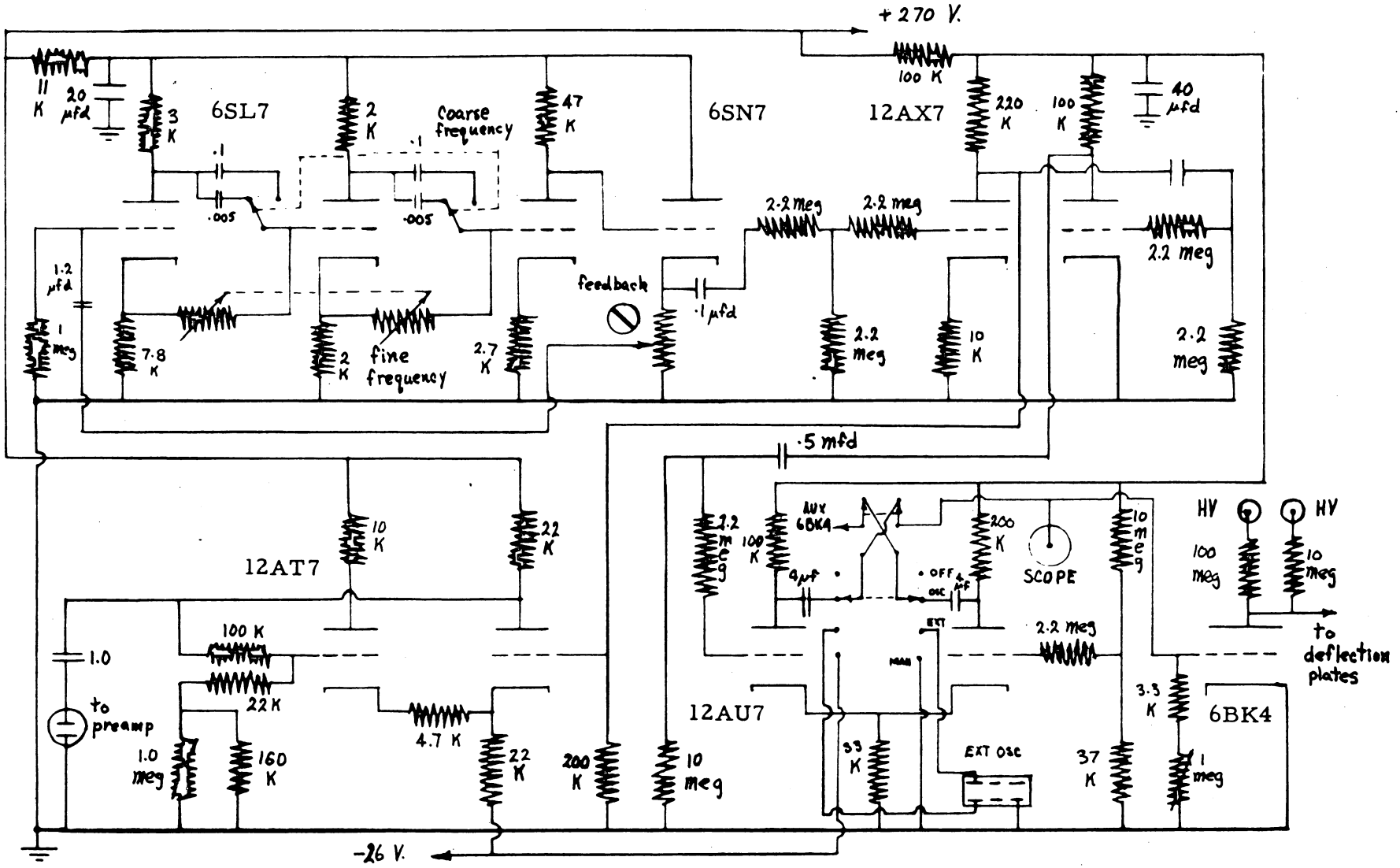

Figure 2 CIRCUIT DIAGRAM OF PULSE CONTROL UNIT

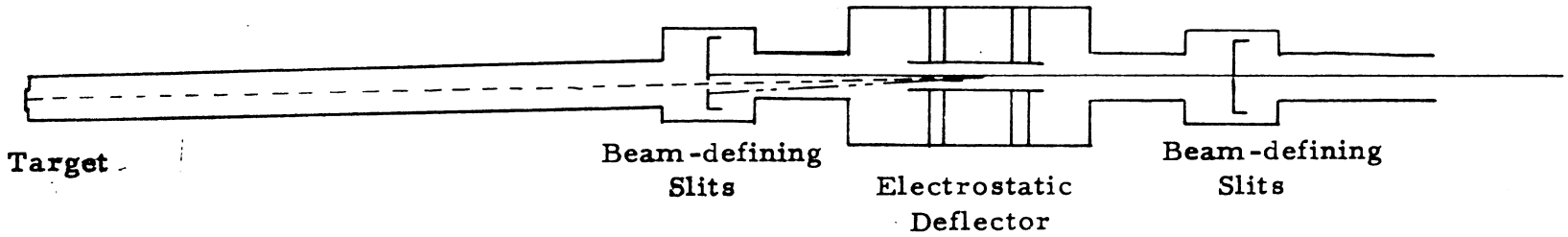

Figure 3 PATH OF BEAM

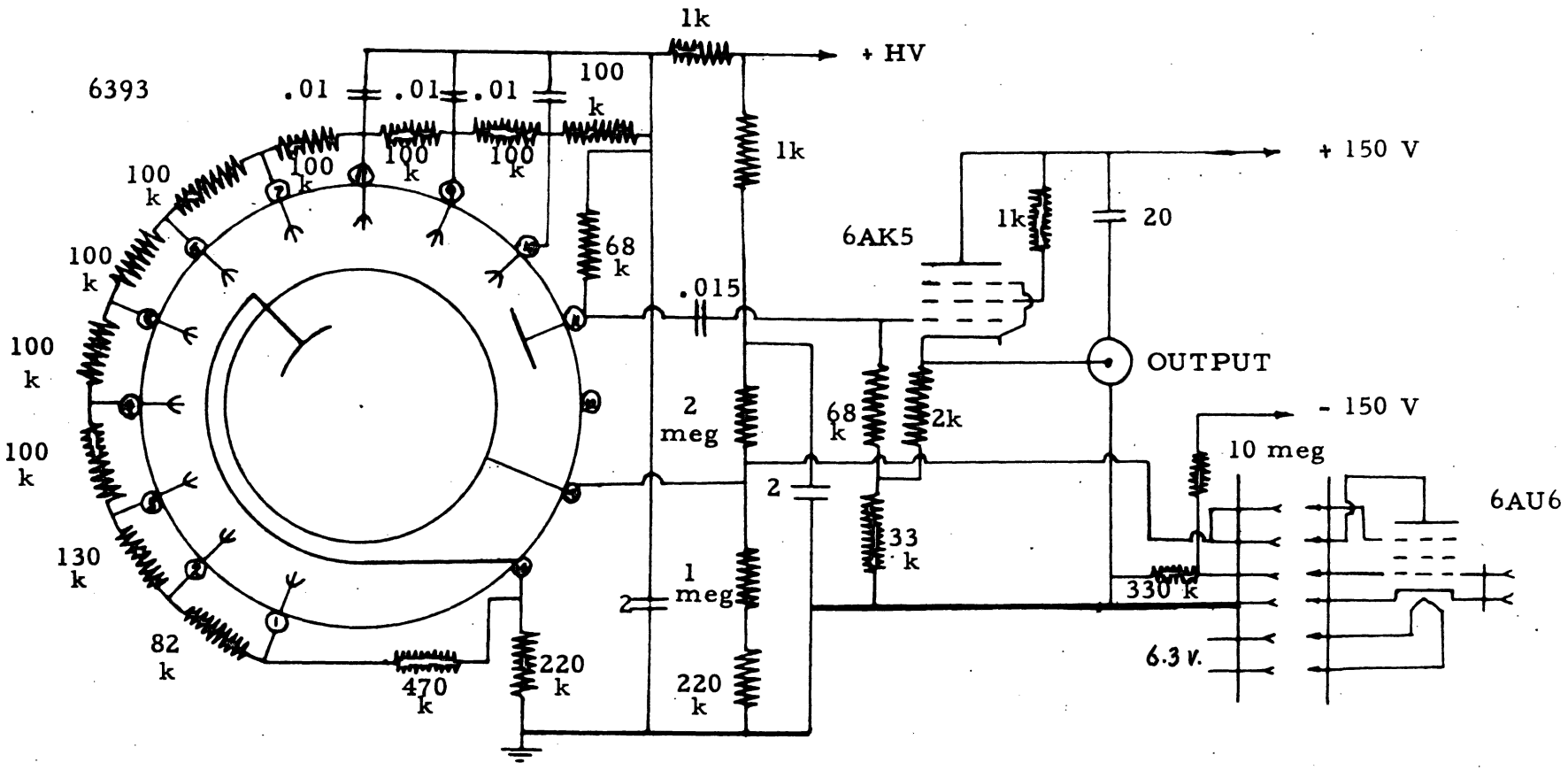

Figure 4 CIRCUIT DIAGRAM OF PREAMPLIFIER

that when it is removed the preamp becomes a conventional one. Having the switch tube confined to a separate chassis has the additional advantage of isolating the strong switching signals from the rest of the preamp. Even then these signals cause trouble and isolating circuits are necessary to reduce these effects.

The lowest frequency obtainable from the control unit generator is about 0.5 cycles per sec. For reasons which will be discussed later it is sometimes desirable to pulse the beam at a considerably slower rate than this. As can be seen from Fig. 2, provisions have been made in the control unit for driving the unit from an external square wave generator. The low frequency square wave generator used to drive the control unit is shown in Fig. 5. It makes use of a circuit for producing the square waves using neon glow lamps in multivibrator type operation.[16] The lower frequency limit of the circuit is determined only by the size of the condenser available. In actual operation a 54 mfd. external capacitor was used to produce square waves with a period of 35 sec. The signal from the neon oscillator is fed to a 6AU6 amplifier and clipper and a 6AQ5 cathode follower. Since the circuits are all direct coupled there is no degeneracy of wave shape with frequency.

The counter assembly consists of a 3" x 3" Harshaw NaI(Tl) scintillation crystal, a 24" lucite light pipe, and a 3" Dumont 6393 photomultiplier. The light pipe is optically coupled to the crystal and phototube and wrapped with 3 mil aluminum foil and black tape so

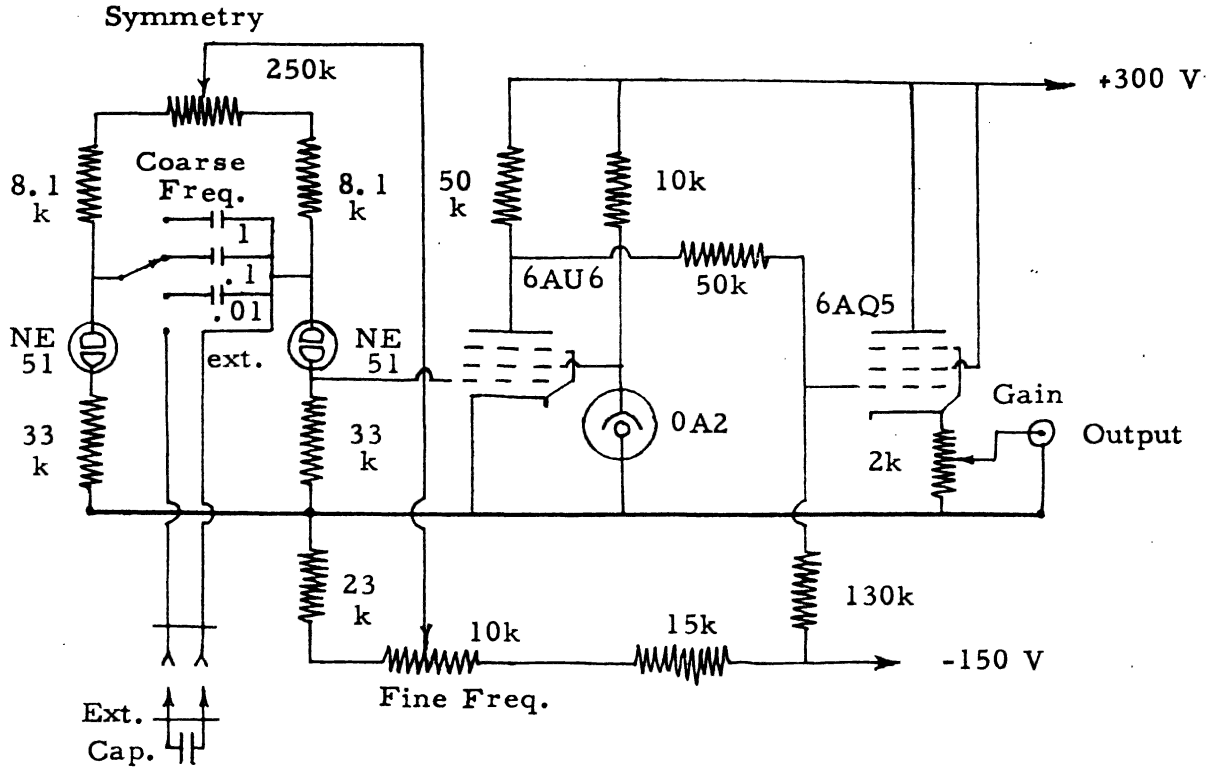

Figure 5 CIRCUIT DIAGRAM OF LOW FREQUENCY SQUARE WAVE GENERATOR

that the whole system is light tight. In this arrangement the system has a resolution of about 12% for the Cs^{137} gamma ray as compared to about 8-1/2% when the crystal is mounted directly on the phototube. Surprisingly, the resolution seems to be independent of the length of the light pipe and to depend only on the number of optical couplings between the crystal and phototube. The phototube is shielded from external fields with a Dumont mu-metal shield. Despite this precaution, there is still an observed gain change of 0.32% in the counting system between the two field directions. As will be discussed later this shift is such that it produces an effect in the opposite direction from the polarization effect for left circularly polarized bremsstrahlung. It would therefore tend to mask any polarization effect, but if one were present it could not be attributed to a field-dependent gain shift in the apparatus.

Both the counter assembly and the analyzing magnet used in the polarization measurement are supported by an aluminum table, as shown in Fig. 6. Notice that the counter assembly is mounted on a long boom projecting behind the magnet.

A very important part in the whole investigation is played by the Radiation Counter Laboratories, Inc. 256 Channel Analyzer. This machine of course is useful in analyzing the counter output pulses, but perhaps its most significant feature is the operation of the "complement" mode. One may make use of this operation to subtract one pulse distribution from another. Using this feature properly one can subtract background leaving only the desired spectrum.

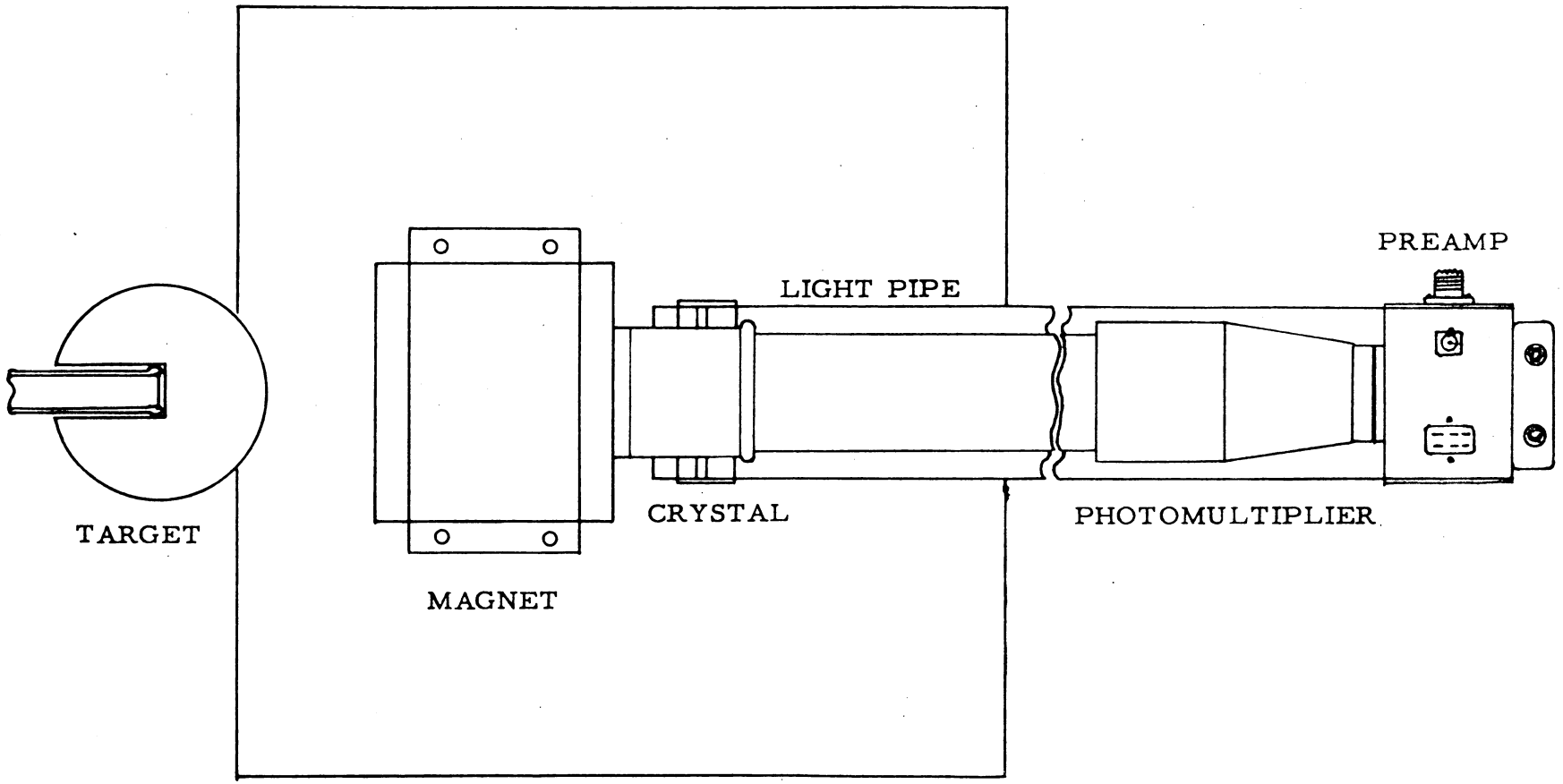

Figure 6 THE COMPTON POLARIMETER

This simplifies the measurement of bremsstrahlung spectra. It is even more useful in the polarization measurements, however, where one is trying to observe a difference in counting rates of something less than 5%. By using the 256 Channel Analyzer one can not only detect polarization but actually get some idea of the degree of polarization as a function of energy. This is done by repeatedly subtracting spectra taken with the field in opposite directions until one is left with a difference spectrum over many runs. From this one can directly determine the polarization function, given sufficiently good statistics.

The table, counter assembly, and magnet, as shown on Fig. 6, along with the magnet power supply constitute the Compton polarimeter. The bremsstrahlung emerging from the paraffin sphere are passed through the core of the magnet and detected by the counter. The magnetic field is reversed and the difference in counting rate is determined, giving a measure of the polarization.

To save time and effort, the power supply and reversing controls of the magnet were located some distance away, at the console of the Van der Graaff. With this arrangement one could alter the field direction without taking the beam off the target or otherwise disturbing the operation.

The design of the analyzing magnet received particular attention due to the critical role it plays in any polarization measurement.

It is shown in Appendix II that for 100% left circularly polarized photons the differential transmission upon field reversal is proportional to Tanh(KL) where K is a constant and L is the magnet thickness. Thus one might suppose that one has only to increase L to obtain greater and greater polarization effects and more sensitive detection. However, if the magnet is too thick the counting rate will be so small that an excessive amount of time will be required to obtain meaningful counting statistics. Even more important in this connection is the background problem. Since this investigation makes use of a nuclear reaction, even with a pulsed beam there is a high background counting rate due principally to neutron induced activity. If the magnet is too thick the small changes in counting rate due to field reversal will be completely swamped by the background. Thus we must maximize the detectable polarization effect, i.e., that which we can observe in the presence of a given background. Appendix II presents a detailed account of this calculation. The results indicate that the optimum magnet thickness is between 10 and 14 cm.. On the basis of this a magnet was constructed which can be assembled to have a core thickness of either 10.2 cm or 12.7 cm. However, for all succeeding measurements the 10.2 core was used. A cross section of the magnet is shown in Fig. 7. The coil is wound with about 1,850 turns of #16 B&S gauge nylon insulated wire. The core diameter is 3", the same size as the NaI crystal.

An investigation was made to determine how much radiation was

CROSS SECTION OF ANALYZING MAGNET

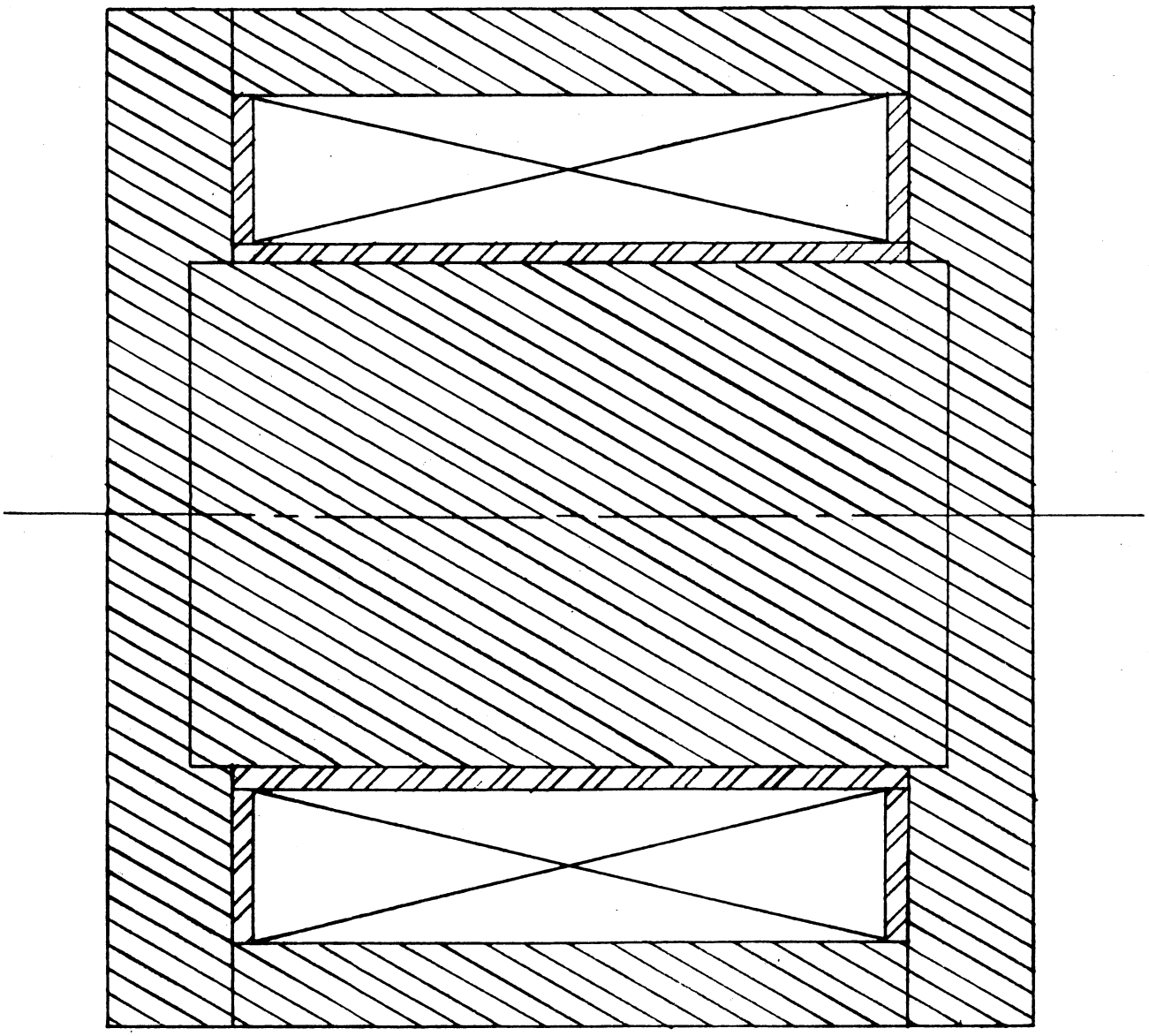

Figure 7

scattered into the counter by the magnet coil, housing, etc.. A ThC" source which emits a 2.6 mev. gamma ray was placed in the position the target ordinarily occupies and a spectral distribution was taken with the radiation passing through the fully assembled magnet and through the core only. The results showed that the counting rate was slightly lower with the full magnet than with the core only, indicating that scattering into the counter is not an important consideration.

III. Experimental Difficulties

The principle experimental difficulty arises from the large background present during the measurements. This background comes partly from the deuterons striking carbon on the beam-defining slits and from extraneous radioactivity made in and around the target. By cleaning the slits and restricting the beam with a tantalum diaphragm most of this background was eliminated.

The other important contribution to the background is due to the radioactivity in the scintillation crystal induced by the prompt neutrons from the $Li^{6,7}(d,n)$ which have energies up to 16 mev.. The principle sources of this radioactivity are F^{20} from the $Na^{23}(n,\alpha)$ reaction, Ne^{23} from the $Na^{23}(n,p)$ reaction, and I^{128} from $I^{127}(n,\gamma)$. These nuclei have half lives of 12 sec., 40 sec., and 25 min., and beta and point energies of 5.3 mev., 4.21 mev., and 2.02 mev., respectively. However, the F^{20} decay is accompanied by the emission of a 1.6 mev. gamma ray, so that the total energy released in the crystal can be as high as 6.9 mev..

By methods discussed below it was determined that for the

bremsstrahlung spectra measurements less than 1% of the counts above 2-1/4 mev. were produced by the background, provided the lead converter was used. However, if the converter was removed so that only the inner bremsstrahlung and the outer bremsstrahlung produced in the target and the paraffin sphere were present then 30% of the counts above 2-1/4 mev. were produced by the background. When the bremsstrahlung was passed through the magnet before counting, these percentages became about 30% and 50% respectively.

In the case of the external bremsstrahlung spectrum measurement, it is possible to subtract most of the background by using the complement mode of the 256 Channel Analyzer. One simply takes a spectrum with the lead converter and paraffin sphere in place and then subtracts off the spectrum taken with the paraffin sphere only.

A more generally applicable method of separating the background was found to be implicit in the beam pulsing technique itself. The calculation in Appendix I shows that in a certain range of pulsing frequency, discrimination between the long and short lived components present in the radioactive decay can be effected. This method can be applied to the present case where all the background decays have markedly longer half-lives than Li^8. As shown in Table I, if we adopt a 100 msec. pulse cycle period we get essentially full yield from all the decays. On the other hand, if we use a 35 sec pulse cycle period we decrease the Li^8 yield by 74% without greatly changing the other yields. Thus if we take a spectrum at the fast pulse rate and

TABLE I

X = Counting Time = Cycle time/2

Radioactive Substance	Half Life (sec)	λ Decay Constant $(sec)^{-1}$	X = 17.5 sec. λX	X = 17.5 sec. Yield $4\bar{R}/Q$	X = 100 msec. λX	X = 100 msec. Yield $4\bar{R}/Q$
Li^8	0.83	8.35×10^{-1}	14.43	0.26	8.35×10^{-2}	1.00
F^{20}	12	5.78×10^{-2}	1.000	0.942	5.78×10^{-3}	1.00
Ne^{23}	40	1.72×10^{-2}	0.299	0.992	1.72×10^{-3}	1.00
I^{128}	1,500	4.62×10^{-4}	7.98×10^{-3}	1.000	4.62×10^{-5}	1.00

subtract a spectrum taken at the slow pulse rate we are left with only 74% of the Li^8 yield and in principle no background. This is what we label the fast-slow pulse technique, and it was used in taking most of the bremsstrahlung spectra presented herein, and to determine the background percentages given above.

Since the continuous bremsstrahlung spectra are measured with a scintillation counter, inevitably there will be some distortion present. Some of this distortion is caused by the energy dependence of the counting efficiency of NaI. In addition, both the crystal and the phototube introduce a certain amount of statistical Gaussian broadening into any distribution. These distortions, however, can be corrected by ordinary numerical corrections.

A more serious type of distortion is introduced by the line shape which is characteristic of the crystal. Due to the processes involved in the detection of gamma rays, there is a finite probability that a gamma ray of given energy will produce a pulse with any height from zero up to a maximum value determined by this energy. Conversely, if we observe a certain size pulse coming from a scintillation counter there is a finite probability that it was produced by any photon having an energy greater than that corresponding to this lower limit. Fig. 8 shows such a probability function for a pulse height corresponding to a 2 mev. photopeak.

Thus the entire spectrum is distorted by this effect, and one must

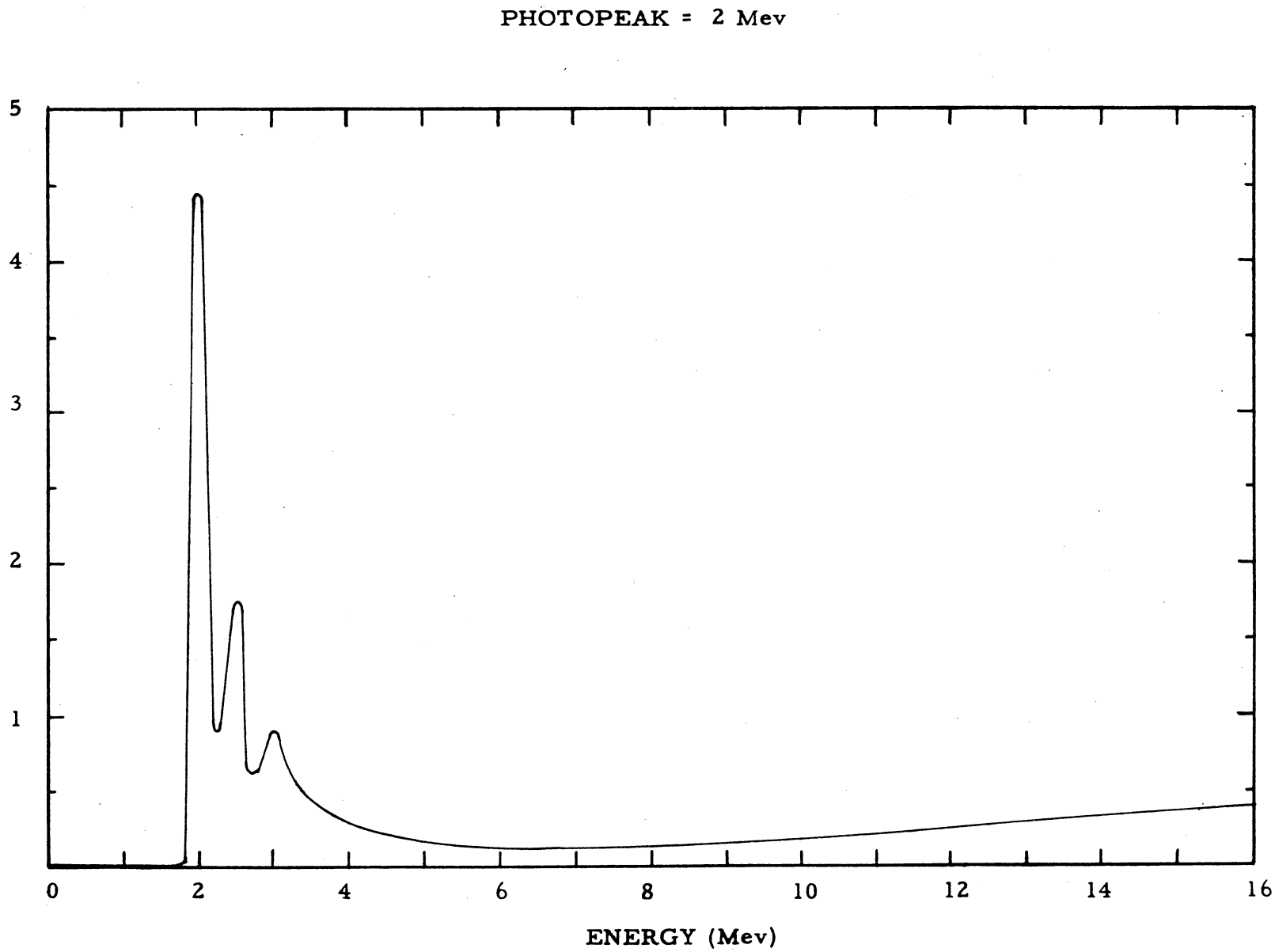

Figure 8 GAMMA RAY PROBABILITY DISTRIBUTION FOR A GIVEN PULSE HEIGHT

resort to special correction techniques to overcome this distortion so that one can meaningfully compare theoretical and experimental gamma ray spectra. These methods require a knowledge of the efficiencies and line shapes at all energies in the range in question. Such a method of allowing for crystal distortion, is discussed in Appendix IV.

IV. Results

A. Bremsstrahlung Spectra.

For purposes of comparison with experiment, both the external and inner bremsstrahlung spectra for Li^8 were calculated (see Appendix III) in accordance with the theories of Bethe and Heitler,[18] and Knipp and Uhlenbeck,[19] respectively. In the former case one radiative collision per electron (thin target) and no screening were assumed, so that the calculated curve is an approximation. Fig. 17 shows these calculated spectra for the inner bremsstrahlung and for the external bremsstrahlung for various thicknesses of lead, aluminum, lithium, and paraffin which correspond to the thicknesses actually present in the experimental measurement.

Fig. 9 shows the experimental and theoretical external bremsstrahlung spectra produced by 0.032" of lead. The dotted curve shows how crystal distortion would be expected to change the theoretical curve on the basis of the calculation in Appendix IV. The crosses represent the external spectrum taken with a fast-slow background subtraction, and the circles represent the spectrum taken by removing the converter for the subtraction. All curves are normalized to coincide at 6 mev.

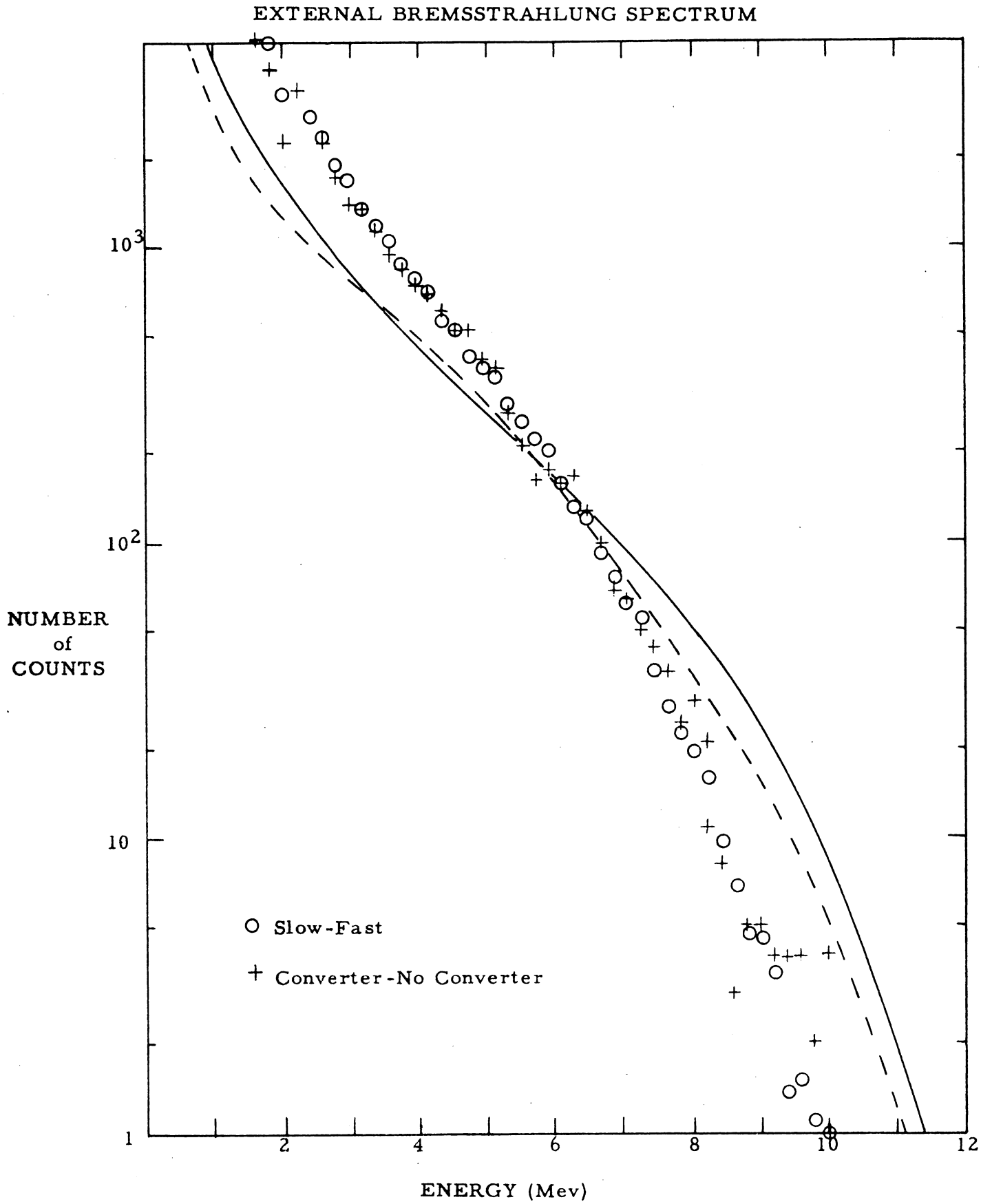
EXTERNAL BREMSSTRAHLUNG SPECTRUM
NUMBER of COUNTS
10^3
10^2
10
1
2
4
6
8
10
12
ENERGY (Mev)
O Slow-Fast
+ Converter-No Converter

Figure 9

There is a very marked difference in slope between the experimental and theoretical results, and this difference is apparently not due to crystal distortion. Moreover, it is not due to effects produced by passing the bremsstrahlung through paraffin since doubling the paraffin thickness leaves the shape of the spectrum unaffected. A possible explanation for this difference may lie in the thick target effects discussed in Appendix III, but it seems unlikely that these would produce a difference as large as that observed. In any case, it is hoped that the differences between the experimental and theoretical spectra can be reconciled by an improved theoretical calculation.

Fig. 10 shows analogous curves taken with no converter. In this case only the fast-slow background subtraction was made. The theoretical curve is the inner bremsstrahlung spectrum calculated in Appendix IV and again the dotted curve is the expected crystal distortion. There may be some objections to comparing the inner bremsstrahlung spectrum to an experimental curve that has an appreciable component of external thick target bremsstrahlung from the paraffin. However, we see from Fig. 17 that the amounts of inner bremsstrahlung and external bremsstrahlung due to paraffin are comparable. Notice the relative intensities which give us some idea of the amount of inner bremsstrahlung that can be expected in a spectrum that is taken without the lead converter. Since screening effects would bring the paraffin curve even lower, one can reasonably expect a sizeable part of such a spectrum to be due to inner bremsstrahlung.

INNER BREMSSTRAHLUNG SPECTRUM

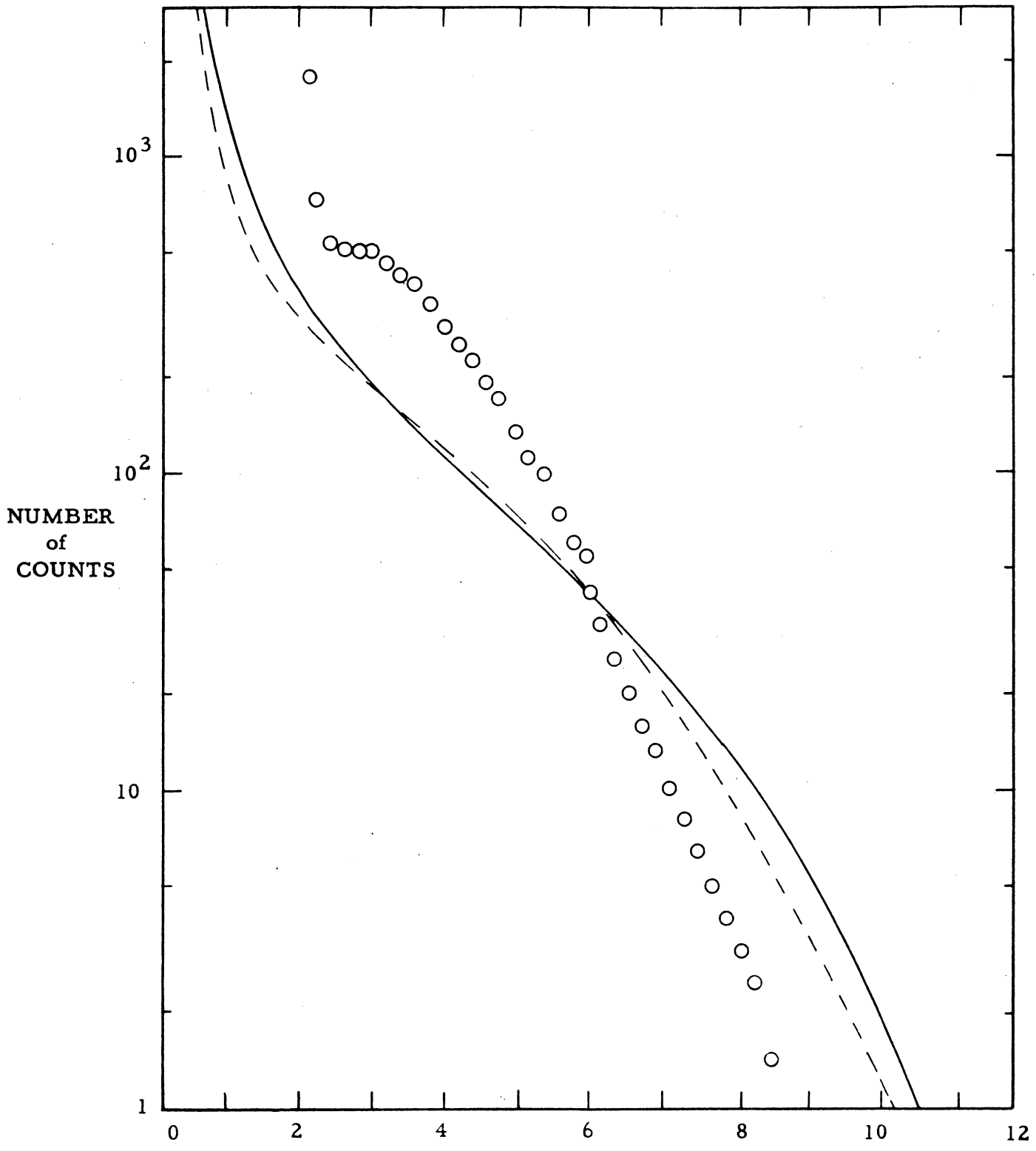

Figure 10

Deviations from theoretical predictions have been observed by Linden and Starfeldt[17] in the spectra of both inner and external bremsstrahlung from the P^{32} beta decay which has an end point energy of 1.70 mev., These deviations are not as pronounced as in our case but it is not unreasonable that they might increase with energy.

B. Polarization

The polarization effect, δ , is defined by:

$$\delta = (T(fr) - T(ff))/(T(fr)+T(ff)).$$

where T(fr) is the transmission with the magnetization parallel to the direction of propagation, and T(ff) is the transmission with the magnetization antiparallel to the direction of propagation of the photons.

Fig. 11 shows the measured values of δ, for external bremsstrahlung at various energies. The horizontal bars indicate the channel width over which the determination was made, and the vertical bars indicate the probable error, i.e. the width of one standard deviation. The curve gives the calculated value of δ for 100% left circular polarization.

Fig. 12 shows the polarization P which is calculated from this by dividing the observed δ by the δ corresponding to 100% polarization. Due to the statistical spread of the points one cannot determine too precisely the shape of the polarization vs energy curve but the indicated curve seems to be a reasonable fit and it agrees with the theory.[2, 3]

Figure 11 POLARIZATION EFFECT vs ENERGY

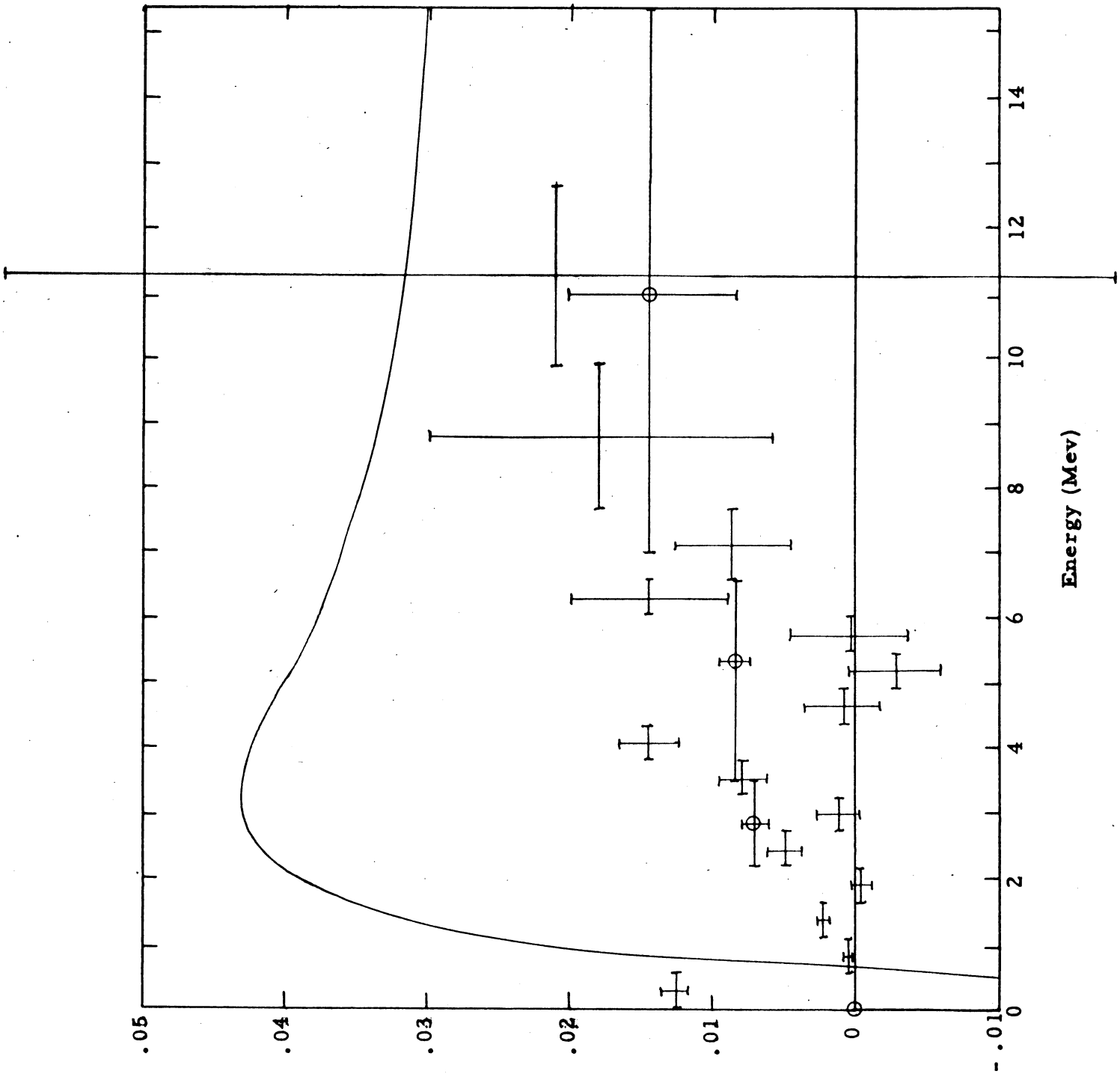

Figure 12 POLARIZATION VS ENERGY

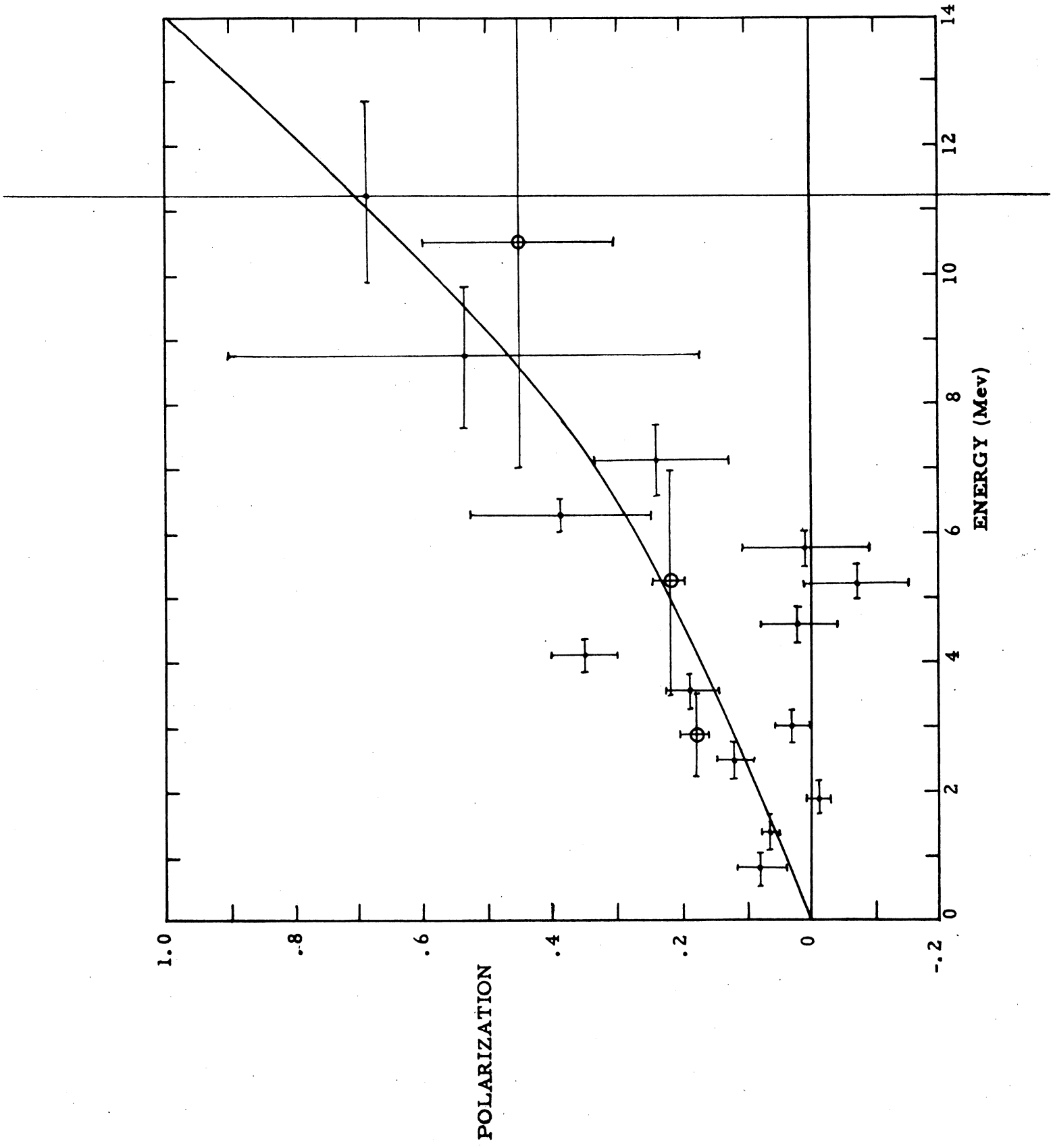

Goldhaber, Grodzins, and Sunyar[4] obtained a similar result for the Sr^{90}-Y^{90} beta decay, with a polarization effect in the same direction as ours. However, if we use the Gunst and Page[8] expression for the polarization effect we are lead to conclude that the experimental effect is in the wrong direction. Since there is no mention of such a conflict in the literature, we must conclude that this difference is a result of a difference in terminology concerning right and left circular polarization. In view of this, throughout this discussion we have used McVoy's definitions, according to which a right circularly polarized photon carries a positive unit of angular momentum in the direction of propagation. Then we must modify the transmission ratio expression of Gunst and Page[8] to read: $T_{lcp}/T_{rcp} = e^{-2NLv\sigma_l}$ This expression leads to a predicted polarization effect in the direction observed.

Although a similar study of polarization was made for the bremsstrahlung spectrum taken without a converter in an effort to measure the polarization of the inner bremsstrahlung, no polarization effect could be observed. However, there is no reason to assume that this is due to any fundamental absence of polarization in the spectrum. Rather we attribute this null result to the fact that the high background will reduce the size of the observable effect so that it will be completely masked by the field dependent gain shift.

V. Conclusion

The results presented herein do not represent the final outcome of the investigations but rather a preliminary report on these investigations. A great deal of time and effort has been devoted to developing the experimental techniques necessary to make these measurements and improvements are still needed in some areas. In addition, more attention must be devoted to calculating the theoretical functions necessary for comparison.

Nevertheless, the principal obstacles seem to have been overcome, and the plan for the future is clear. The inner bremsstrahlung measurements need more refinement, but more important, other decays are to be studied, particularly the B^8 positron decay which should be very similar to that of Li^8 except that the external bremsstrahlung polarization should be in the other direction, and the N^{12} positron decay with a 17 mev. end-point energy which should make any electron shower effects more pronounced.

However, as it stands we have established that the polarization of the Li^8 external bremsstrahlung agrees in energy dependence and direction with the predictions of the two-component neutrino[1] theory and the calculations of McVoy[2] and of Fronsdal and Überall[3] as well as the experimental results for lower energy beta decays.[4, 5, 6, 7] In addition we have found certain disagreement between theory and experiment for both inner and external bremsstrahlung spectra, although admittedly it is difficult to ascertain the significance of this

result without further calculation and, in the inner bremsstrahlung case, more refined experiments.

Appendix I

Yield Calculation for a Pulsed Beam

Let Q = Number of atoms/sec. produced by the beam.

λ = Decay constant = 0.693/half-life

X = Bombarding period

Y = Counting period

Z = Cycle period = $X + Y$

$N(t)$ = Number of Atoms present at time t

C_n = Number of disentegration occurring in the n^{th} counting interval.

Now $N_{x1} = N(t = x) = \frac{Q}{\lambda}(1-e^{-\lambda x})$

$N_{y1} = N(t = z) = N_{x1}\, e^{-\lambda y} = \frac{Q}{\lambda}(1-e^{-\lambda x})\, e^{-\lambda y}$

$C_1 = N_{x1}(1-e^{-\lambda y}) = \frac{Q}{\lambda}(1-e^{-\lambda x})(1-e^{-\lambda y})$

$N_{x2} = N_{y1}e^{-\lambda x} + N_{x1} = \frac{Q}{\lambda}(1-e^{-\lambda x})(1 + e^{-\lambda z})$

$C_2 = \frac{Q}{\lambda}(1-e^{-\lambda x})(1-e^{-\lambda y})(1 + e^{-\lambda z})$

Then the nth terms are:

$$N_{xn} = \frac{Q}{\lambda}(1-e^{-\lambda x})(1 + e^{-\lambda z} + e^{-2\lambda z} + \ldots + e^{-n\lambda z}) = \frac{Q}{\lambda}(1-e^{-\lambda x})\sum_{m=0}^{n} e^{-\lambda m z}$$

$$C_n = \frac{Q}{\lambda}(1-e^{-\lambda x})(1-e^{-\lambda y})\sum_{m=0}^{n} e^{-\lambda m z}$$

In the limit as $n \longrightarrow \infty$ these become:

$$N_{x\infty} = \frac{Q}{\lambda}\,\frac{1-e^{-\lambda x}}{1-e^{-\lambda z}} \qquad C_\infty = \frac{Q}{\lambda}\,\frac{(1-e^{-\lambda x})(1-e^{-\lambda y})}{1-e^{-\lambda z}}$$

Setting $X = fz$ $\quad Y = \bar{f}z$ $\quad$ so that $f + \bar{f} = 1$

we get $N_{x\infty} = \frac{Q}{\lambda}\,\frac{1-e^{-\lambda f z}}{1-e^{-\lambda z}} \qquad C_\infty = \frac{Q}{\lambda}\,\frac{(1-e^{-\lambda f z})\,(1-e^{-\lambda \bar{f} z})}{1-e^{-\lambda z}}$

Now we wish to maximize the disintegration per unit time for both f and z. We must therefore maximize $C_\infty/z = R$

First consider the f dependence:

$$\frac{\partial R}{\partial f} = \frac{\Omega}{\lambda z}\frac{\partial}{\partial f}\frac{(1-e^{-\lambda fz})(1-e^{-\lambda \bar{f} z})}{1-e^{-\lambda z}}$$

$$= \frac{\Omega}{\lambda z}\frac{\lambda z\left[e^{-\lambda fz}(1-e^{-\lambda \bar{f} z}) - e^{-\lambda \bar{f} z}(1-e^{-\lambda fz})\right]}{1-e^{-\lambda z}}$$

$$= \Omega\,\frac{e^{-\lambda fz} - e^{-\lambda \bar{f} z}}{1-e^{-\lambda z}}$$

Setting $\frac{\partial R}{\partial f} = 0$ we see that if $z \neq 0$ we must have:

$$e^{-\lambda fz} = e^{-\lambda \bar{f} z} \quad \text{or} \quad f = \bar{f} = \frac{1}{2}$$

Thus $X = Y = \frac{1}{2}z$

Then $\bar{R} = \frac{\Omega}{2\lambda x}\frac{1-e^{-\lambda x}}{1+e^{-\lambda x}}$

Now maximize $\bar{R}$ with respect to X:

$$\frac{\partial \bar{R}}{\partial x} = \frac{\Omega}{2\lambda}\frac{\partial}{\partial x}\frac{1}{x}\frac{1-e^{-\lambda x}}{1+e^{-\lambda x}}$$

$$= \frac{\Omega}{2\lambda}\left[\frac{\lambda x e^{-\lambda x} + \lambda x e^{-2\lambda x} - 1 + e^{-2\lambda x} + \lambda x e^{-\lambda x} - \lambda x e^{-2\lambda x}}{x^2(1+e^{-\lambda x})^2}\right]$$

$$= \frac{\Omega}{2\lambda x^2(1+e^{-\lambda x})^2}(e^{-2\lambda x} + 2\lambda x e^{-\lambda x} - 1)$$

Setting $\frac{\partial R}{\partial x} = 0$ we see that if $X \neq \infty$ we must have:

$$e^{-2\lambda x} + 2\lambda x e^{-\lambda x} - 1 = 0$$

$$\text{or } e^{-\lambda x} = -\lambda x \pm \sqrt{1+\lambda^2 x^2}$$

Since $e^{-\lambda x}$ cannot be negative and since $\lambda x \geq 0$ we must take the positive root.

so $e^{-\lambda x} = \sqrt{1+\lambda^2 x^2} - \lambda x$

This equation is satisfied only at $\lambda x = 0$ and $\lambda x \to +\infty$. We therefore conclude that there are no intermediate maxima.

We can evaluate the function $\bar{R}/\Omega$:

The asymptotic forms are: $\bar{R}/\Omega = \frac{1}{2\lambda x} \frac{1-e^{-\lambda x}}{1+e^{-\lambda x}} \longrightarrow 1/4$ as $X \longrightarrow 0$

$\longrightarrow \frac{1}{2\lambda x}$ as $X \longrightarrow \infty$

λX	$\bar{R}/\Omega$
0	.2500000
.01	.2499935
.1	.249793
.2	.249170
.3	.248142
.4	.246718
.6	.242760
.8	.237468
1.0	.231059
1.5	.211716
2.0	.190398
3.0	.150858
4.0	.120503
6.0	.082921
8.0	.062458
10.0	.049995
15.0	.033333
20.0	.025000
....	.....

Thus we may conclude that if one has $\lambda x < 1$ then the yield is essentially at saturation. If, as in our case, $x = 100$ msec. $= 10^{-1}$ sec.

$\lambda(Li^8) = 8.35 \times 10^{-1}$ sec^{-1} $\quad \therefore \lambda x = 8.35 \times 10^{-2}$; $\bar{R} \cong \Omega/4$

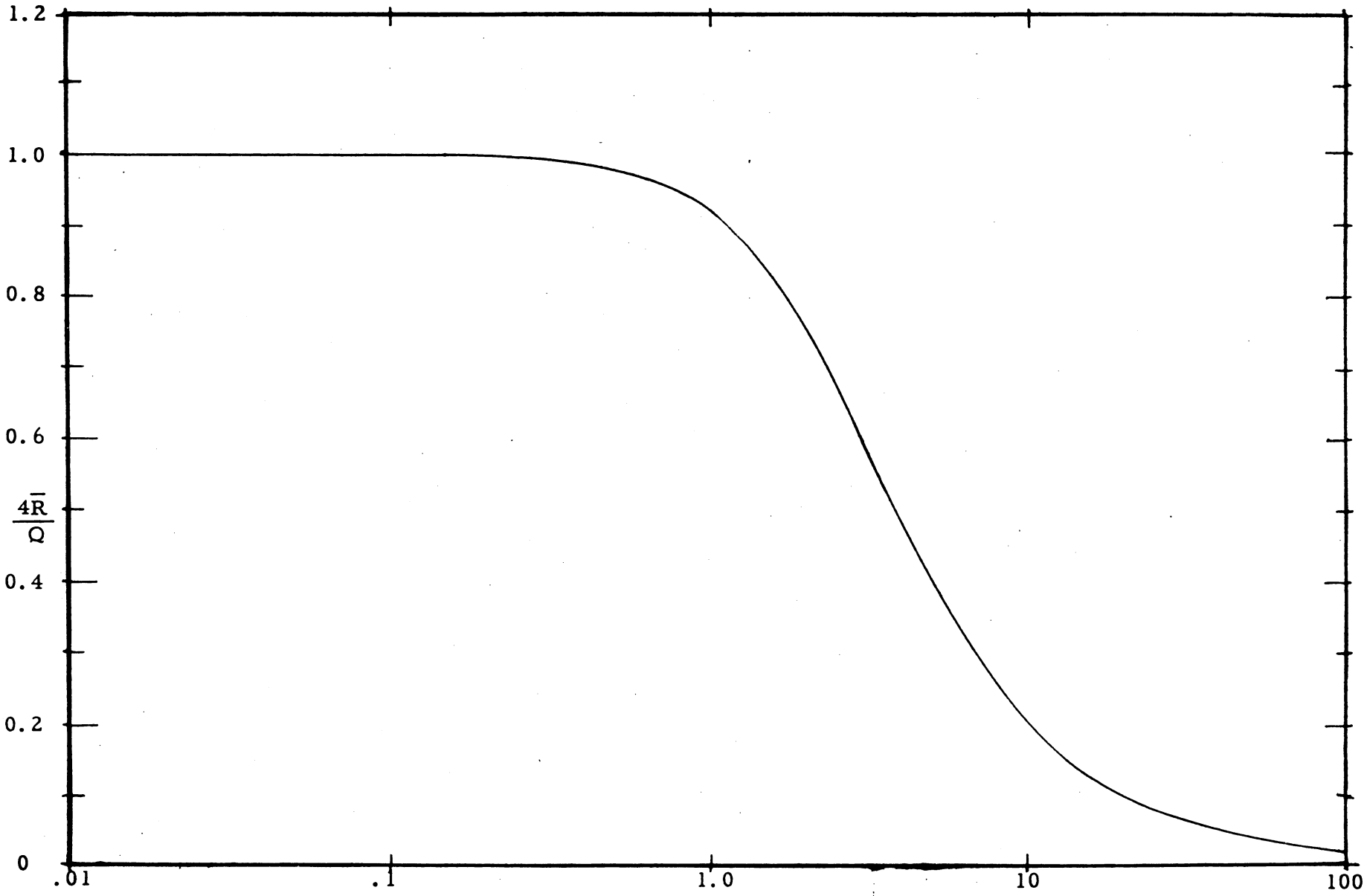

Fig. 13

Appendix II

MAGNET OPTIMIZING CALCULATION

The differential cross section for Compton scattering is given by Gunst and Page[8] as:

$$\frac{do}{dW} = \frac{1}{2} r_o^2 \frac{k^2}{k_o^2} \left\{ \left(\frac{k_o}{k} + \frac{k}{k_o} \sin^2 \theta \right) \mp \left(\left(\frac{k_o}{k} - \frac{k}{k_o} \right) \cos\theta \cos\Psi + \left(1 - \frac{k}{k_o} \right) \sin\theta \sin\phi \sin\Psi \right) \right\}$$

where $r_o = e^2/m_o c^2$, $dW = \sin\theta \, d\theta \, d\phi$, and Ψ = angle of electron with polar axis. The upper sign in the equation corresponds to right circular polarization (in McVoy's[2] terminology).

Let us consider this expression as two cross sections, one independent and one polarization dependent: $\sigma = \sigma_o \pm \sigma_1$ with the sign convention as before. Upon integration over θ and ϕ we find that:

$$\sigma_1 = 2\pi r_o^2 \cos\Psi \left\{ \left(\frac{5\gamma^2 + 4\gamma + 1}{\gamma (2\gamma + 1)^2} \right) - \frac{\gamma + 1}{2\gamma^2} \ln (2\gamma + 1) \right\}$$

where $\gamma = k_o / m_o c^2$.

Fig. 14 is the computed curve for o_1 with $\Psi = 0$ (field forward). Notice that above about 0.63 mev. o_1 is negative.

The polarization effect, $\delta = \frac{T(fr) - T(ff)}{T(fr) + T(ff)}$, can be written in terms of σ_1 as:

$$\delta = \frac{e^{-NL(z\sigma_o + \sigma_2 + v\sigma_1)} - e^{-NL(zo_o + o_2 - vo_1)}}{e^{-NL(zo_o + o2 + vo_1)} + e^{-NL(zo_o + o_2 - vo_1)}}$$

$$= \frac{e^{-NLv\sigma_1} - e^{NLv\sigma_1}}{e^{-NLv\sigma_1} + e^{NLv\sigma_1}} = \tanh(-NLv\sigma_1)$$

However, the presence of background prevents δ from being observed directly, and the observable quantity is: $\delta_1 = \delta \frac{I}{I+B} = \delta \frac{I_o T}{I_o T + B}$ $= \delta \frac{RT(nf)}{1 + RT(nf)}$ where I = gamma ray intensity, B = background intensity,

POLARIZATION-DEPENDENT CROSS SECTION VS ENERGY

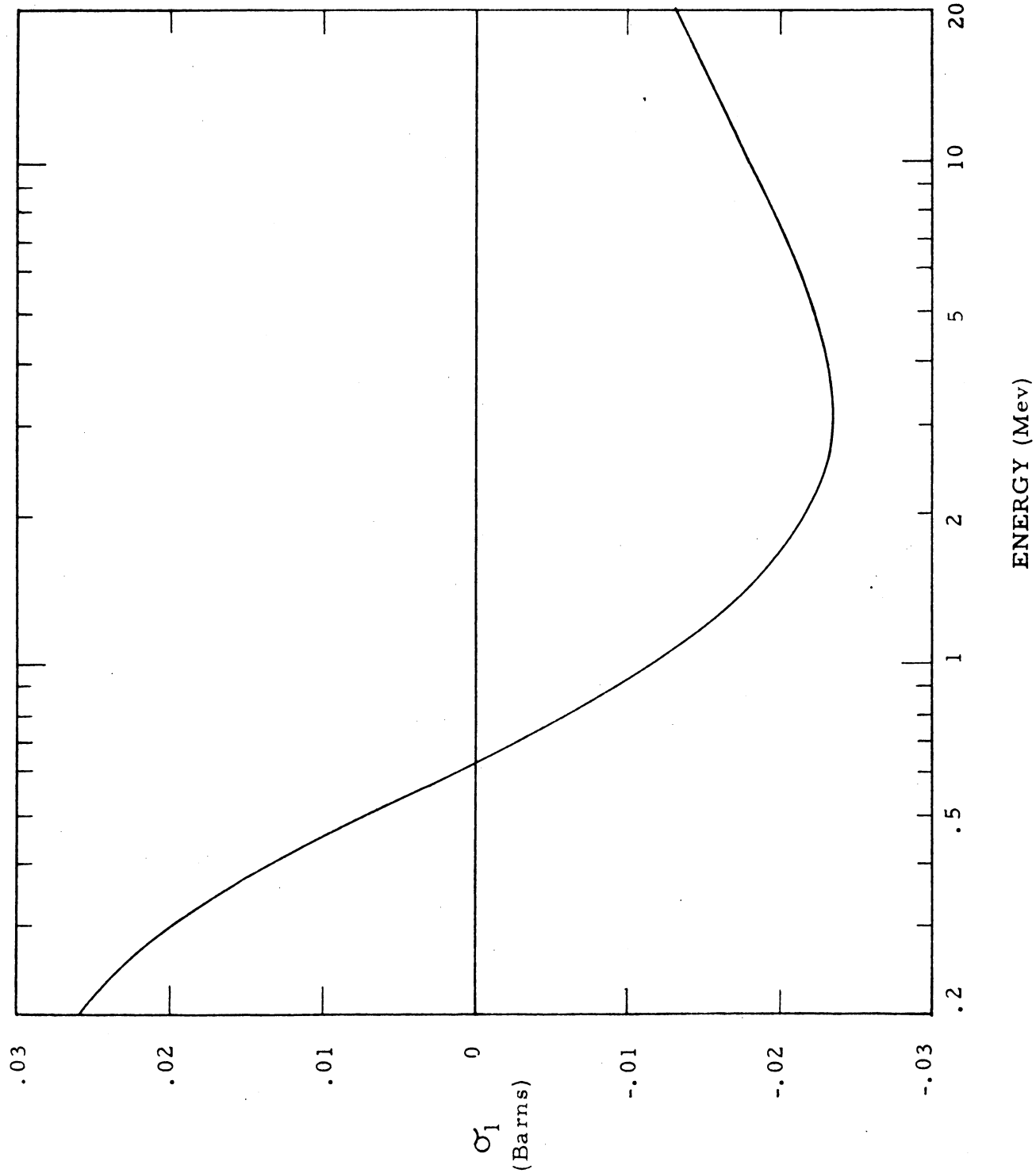

Figure 14

I_o = initial gamma ray intensity, T(nf) = transmission (no field), and $R = I_o/B$. It is important to note that R is the background ratio before the gamma rays are passed through the magnet.

Now $T(nf) = e^{-NL(\sigma_o Z + \sigma_2)} = e^{-sL}$ where σ_2 = cross section due to processes other than Compton scattering and $s = (\sigma_o + \sigma_2)N$. Moreover, if σ_1 is small then $\delta = 1 - e^{2NL\sigma_1 v} = 1 - e^{s_1 L}$ where $s_1 = 2N\sigma_1 v$.

Then $$\delta_1 = \frac{R\, e^{-sL}(1 - e^{s_1 L})}{1 - Re^{-sL}} = \frac{1 - e^{s_1 L}}{1 - e^{sL}/R}$$

The function δ_1 was calculated (by hand) for gamma ray energies of 1/2, 1, 2, 4, 6, 8, 10, 12, and 14 mev; R values of 2, 5, 10, 20, 50, 100, and ∞; and L values of 4, 8, 12, 16, and 20 cm. From this calculation a curve of L_m vs R was plotted which is shown in Fig. 15. Notice that the curves corresponding to the various energies are virtually the same down to about 6 mev. but at lower energies are considerably different. If we expect a background ratio R between 10 and 100 then the magnet should be between 9 and 16 or more conservatively, between 10 and 14 cm. Fig. 16 shows a plot of δ_1 vs energy for L = 10 and 14, and R = 10, 20, 50, and 100. As one would expect the smaller thickness is more favorable for low R values and the larger more favorable for high R values. On this basis the analyzing magnet was designed so that it could be assembled with a length of 10.16 or 12.70 cm..

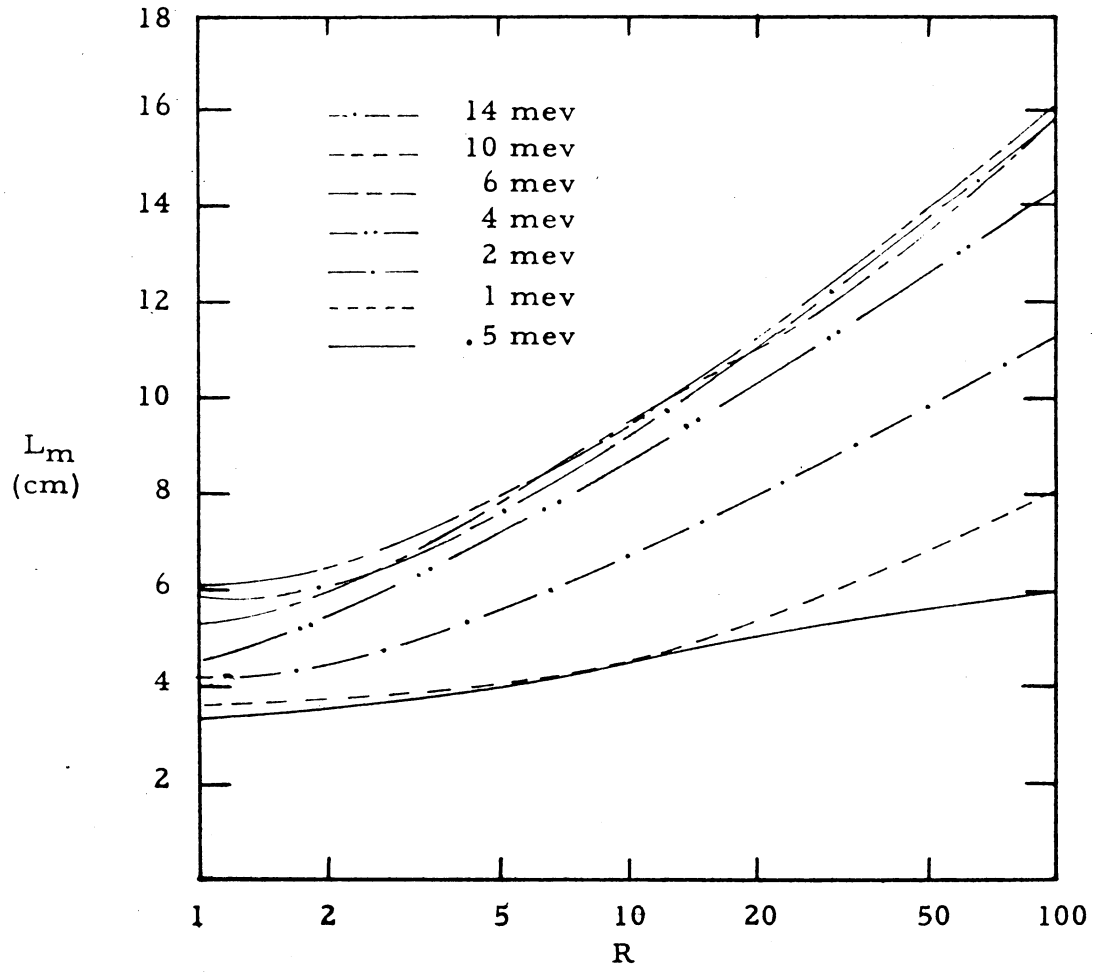

Figure 15 OPTIMUM MAGNET THICKNESS VS BACKGROUND RATIO

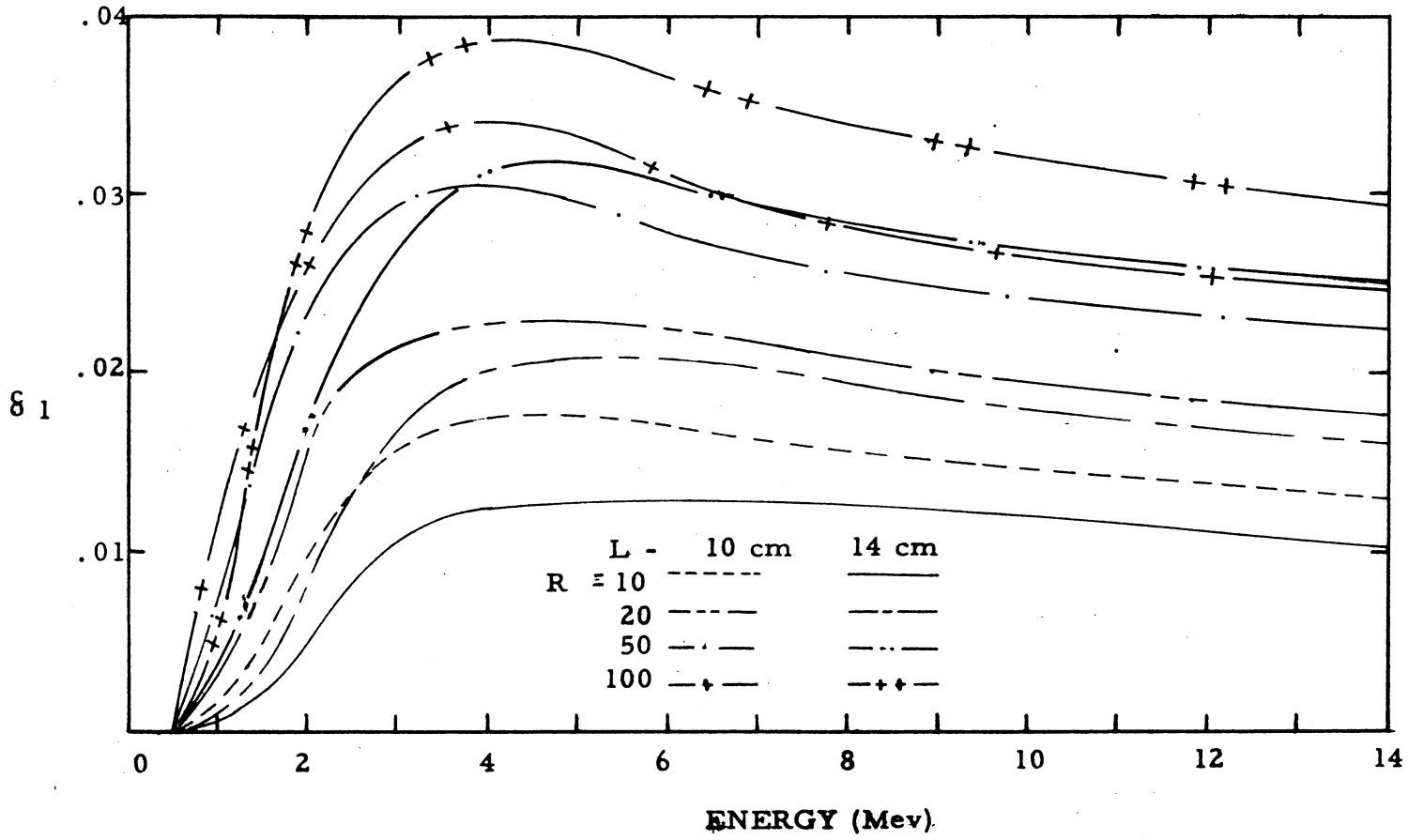

Figure 16 POLARIZATION EFFECT VS ENERGY

Appendix III

CALCULATION OF INNER AND EXTERNAL BREMSSTRAHLUNG SPECTRA

The theoretical inner bremsstrahlung spectrum was calculated on the basis of the results of Knipp and Uhlenbeck.[19] They obtain an expression for the probability of Φ_i of producing a gamma ray during beta emission. This probability function is:

$$\Phi_i = \frac{\alpha p}{\pi p_e k}\left(\frac{W_e^2 - W^2}{W_e p} \ln(W + p) - 2\right)$$

where W_e = initial beta energy; W = final beta energy; k = γ energy = $W_e - W$; P_e = initial beta momentum; p = final beta momentum; and α = fine structure constant = 1/137. All energies are in units of $M_o C^2$, and all momenta are in units of $M_o C$. The probability function has only two independent variables, and we shall take W_e and k as these variables. We can make this dependence explicit by writing:

$$\Phi_i(W_e, k) = \frac{\alpha}{\pi k}\left\{\frac{W_e^2 - (W_e - k)^2}{W_e\sqrt{(W_e - k)^2 - 1}} \ln\left(W_e - k - \sqrt{(W_e - k)^2 - 1}\right) - 2\right\}$$

To obtain the inner bremsstrahlung spectrum from this function we must multiply it by the beta energy distribution and integrate over energy:

$$S_i(k) = \int_{1+k}^{W_o} \Phi_i\ (W_e, k)\ P(W_e)\, dW_e$$

where $S_i(k)$ = inner bremsstrahlung spectrum; W_o = beta end-point energy; and $P(W_e)\, dW_e$ = beta energy distribution.

The theoretical external bremsstrahlung expressing was calculated on the basis of the theory of Bethe and Heitler.[18] They derive a very complicated expression for the probability of producing a γ when a beta is in the field of a nucleus. However, when the initial and final beta

energies and the γ energy are large compared with $m_o c^2$ the probability reduces to:

$$\Phi_e = \frac{4\alpha r_o^2 Z^2}{k W_e^2} (We^2 - W^2 - 2WW_e/3) (\ln(2WWe/k) - 1/2)$$

where r_o = classical electron radius; Z = atomic number of nucleus; and the other symbols have the same meaning as before. This expression can be made an explicit expression of W_e and k by writing it as:

$$\Phi_e(W_e, k) = \frac{4}{3} \alpha r_o^2 Z^2 (4 - 4k/W_e + 3(k/W_e)^2) (\ln \frac{2W_e^2}{k}(1 - k/W_e) - 1/2)$$

As before, the external bremsstrahlung spectrum is obtained from this function by multiplying it by the beta spectrum and integrating over energy:

$$S_e(k) = \int_{1+k}^{W_o} NL\Phi e(We, k)\, P(W_e)\, dW_e$$

where N = atomic density; and L = thickness of material.

This treatment of external bremsstrahlung does not consider screening effects and thus is really an asymptotic expression which becomes better with increasing beta energy. Wheeler and Lamb have investigated the validity of the approximation and find that for a Z of 1, W_e must be 87 mev. to obtain 90% of the yield predicted by the asymptotic expression, but if Z is 92 a W_e of only 19.3 mev. is required. Since the Z of our converter is 82 and the most energetic betas from Li^8 are less than 14 mev. we have reason to suspect the calculation. Their calculations also show that a 1.5% correction should be made for radiation in the field of atomic electrons, but we may safely disregard this.

In addition, the treatment is valid only for thin target bremsstrahlung, i.e. the assumption is made that each electron makes only one radiative collision and no allowance is made for the fact that the beta spectrum is degraded in passing through the target material. It was found experimentally that the spectrum is significantly degraded after passing through only 0.01" of lead. After passage through our 0.032" lead converter the intensity of the spectrum was cut almost in half and also shifted about 12% lower in energy. Thus we would only expect 3/4 of the yield predicted by a thin target calculation and also some shift toward lower energies which would produce an increase in slope. Thus the external bremsstrahlung calculation is highly approximate.

The beta spectrum used in the calculations was obtained from the results of Hornyak and Lauritzen.[20] The calculations were programmed in BELL language and run on the IBM computer at the Shell Oil Company technical services computation laboratory.

For the calculation, four different targets were assumed: 0.5 cm of Li, 3.0 cm of paraffin, 0.1 cm of Al, and 0.032" of Pb. These thicknesses roughly correspond to the effective thicknesses of material present in the experiment. It was determined experimentally that the beta spectrum was virtually reduced to zero after passage through 3 cm of paraffin, so this effective thickness was used instead of 2-1/2". The thicknesses of Li and Al are greater than those present but these values were taken

to emphasize this contribution. The results of the calculation are shown in Fig. 17.

CALCULATED BREMSSTRAHLUNG SPECTRA

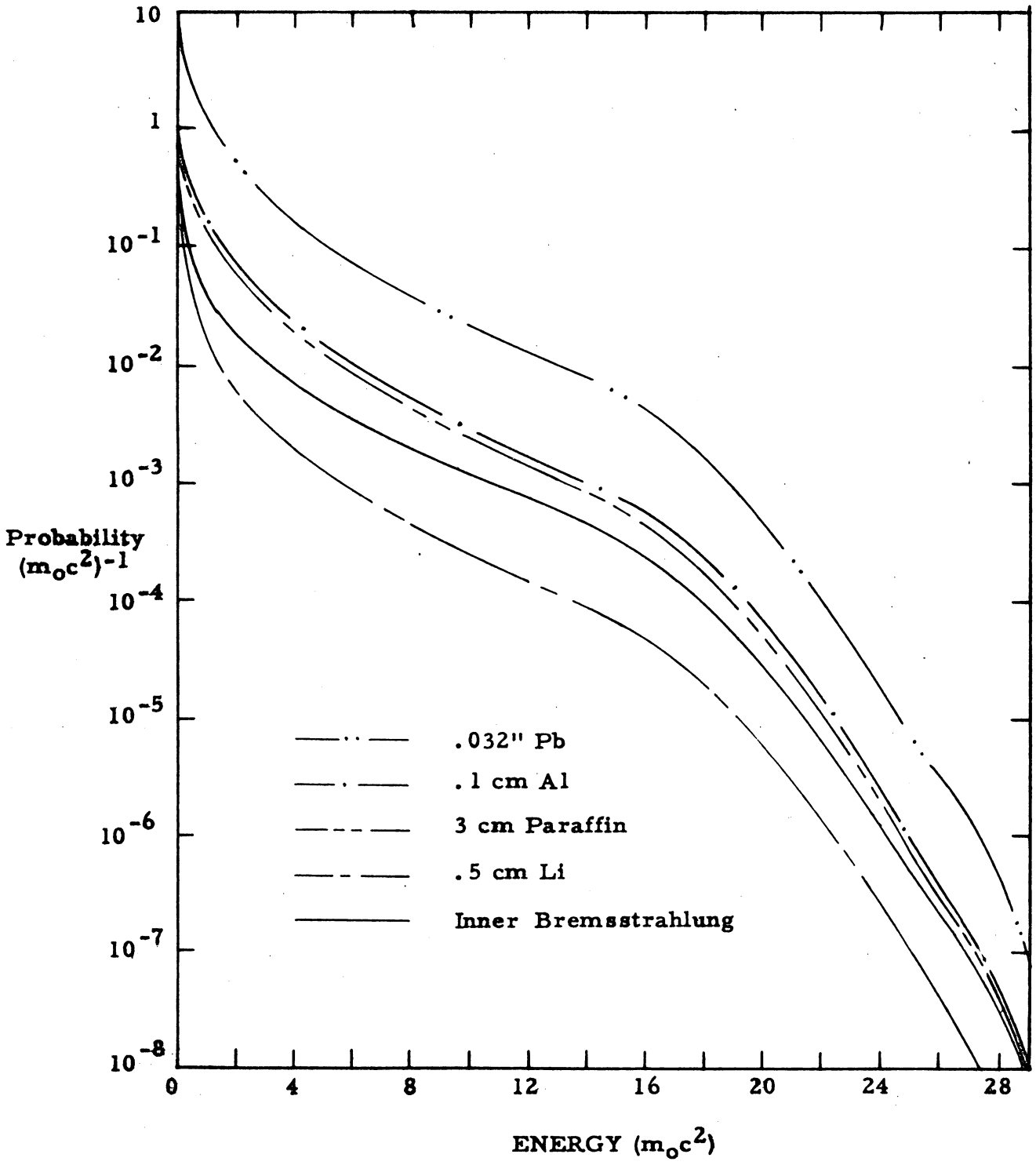

Figure 17

Appendix IV

A METHOD FOR INTRODUCING THE EFFECTS OF CRYSTAL DISTORTION INTO CALCULATED SPECTRA

Any technique which effectively corrects for crystal distortion requires some knowledge of crystal efficiency and the shapes of line spectra. In this treatment, the efficiency was obtained from the gamma ray attenuation coefficient given by Evans[21] and the line shapes were gathered from theoretical[22, 23, 24] and a few experimental[24, 25] sources, since the former are available at a wider variety of energies than experimental line spectra, and also are less ambiguous. Unfortunately, most of these calculated spectra are for crystals other than 3" x 3", so that a good deal of interpolation is necessary.

After these line spectra are obtained, they are normalized to the crystal efficiency and then cross-plotted to give the functions such as that shown in Fig. 8. Each of these functions is associated with a certain pulse height "energy", k'. This is not really the energy of the pulse height, but the energy of the gamma ray whose photopeak is centered at that pulse height. Each of these functions represents the probability that a gamma ray of energy k will result in the production of the pulse height k'. The effect of the crystal distortion on a given gamma ray distribution is described by the integral equation: $\int F(k, k') T(k)dk = S(k')$ The functions we now have correspond to $F(k, k')$ for a given value of k'.

We now take each of these functions and multiply them point by point by the theoretical gamma ray distribution, $T(k)$. These functions are then graphically integrated using a planimeter, giving values of the function $S(k')$ for the value of k' associated with the particular curve. The

correction factor S(R)/T(k) is shown in Fig. 18 where the functions are normalized so that this factor is equal to one at 6 mev. It should be pointed out that this correction factor is not generally applicable and should be used only for the T(k) curve from which it is derived.

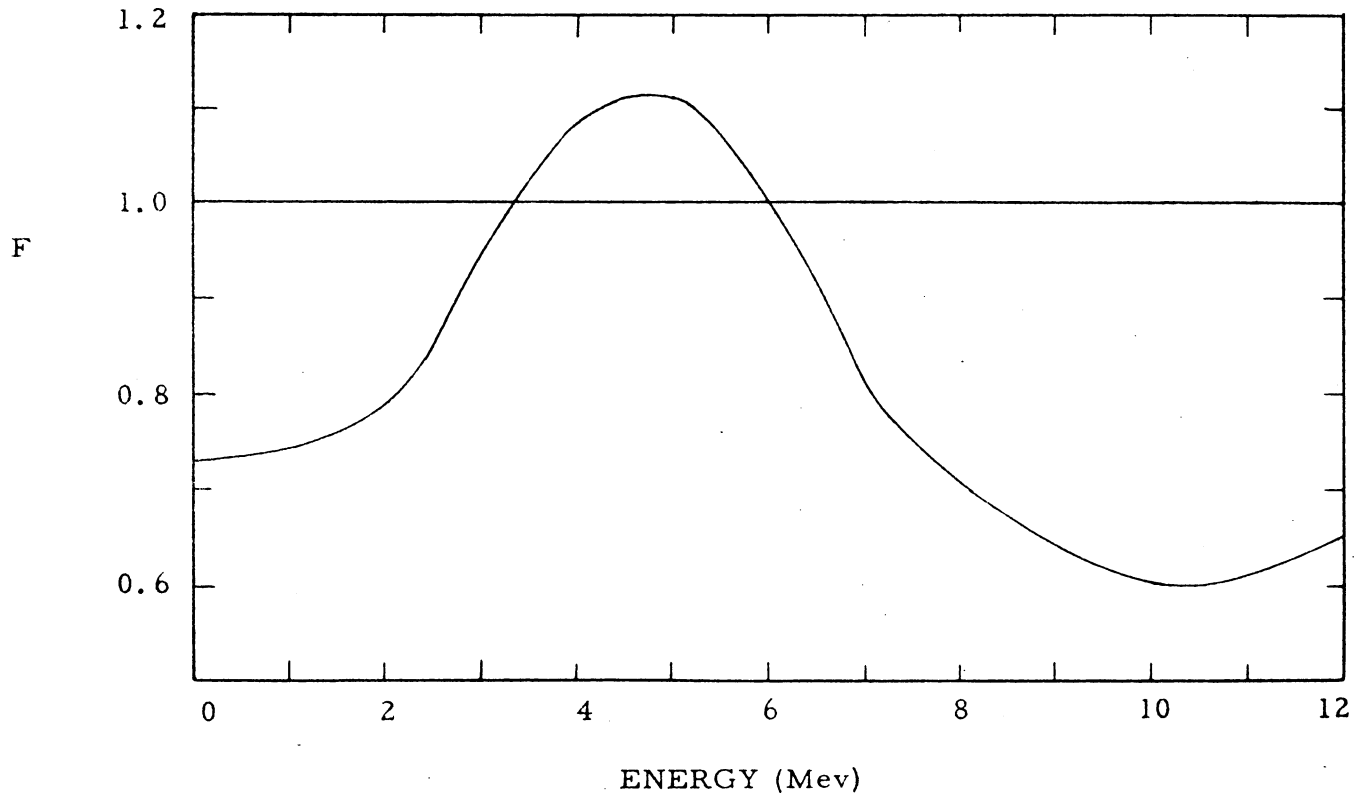

Figure 18 CORRECTION FACTOR VS ENERGY

ACKNOWLEDGMENT

The author wishes to thank Dr. C. M. Class for his guidance and assistance in the course of this project. He would like to thank the staff of the Rice Institute Physics Shop for their aid in building essential experimental apparatus. He is indebted to Mr. B. J. Farmer for assistance in the use of pulsed-beam technique. In addition, he wishes to thank his mother, Mrs. J. G. Cramer, Sr. for her untiring efforts in the preparation of this Thesis.

J. G. C.

BIBLIOGRAPHY

1. T. D. Lee and C. N. Yang, Phys. Rev. 105, 1671 (1957)
2. K. McVoy, Phys. Rev. 106, 828 (1957)
3. Fronsdal and Überall, Phys. Rev. 111, 580 (1958)
4. Goldhaber, Grodzins, and Sunyar, Phys. Rev. 106, 826 (1957)
5. Galster and Schopper, Phys. Rev. Letters 1, 330 (1958)
6. Schopper and Galster, Nuclear Physics 6, 125 (1958)
7. Bisi and Zappa, Phys. Rev. Letters 1, 332 (1958)
8. Gunst and Page, Phys. Rev. 92, 970 (1953)
9. Boehm and Wapstra, Phys. Rev. 109, 456 (1958)
10. Burgy, Epstein, et al, Phys. Rev. 107, 1731 (1957)
11. Goldhaber, Grodzins, and Sunyar, Phys. Rev. 109, 1015 (1958)
12. Hermansfeldt, Maxon, Stahelin, and Allen, Phys. Rev. 107, 641 (1957)
13. Pytte, Phys. Rev. 107, 1681 (1957)
14. S. Rusk, Master's Thesis, Rice Institute (1955)
15. Fornelli and Nalvano, Rev. Sci. Inst. 29, 699 (1958)
16. J. Cramer, Senior Thesis, Rice Institute (1957)
17. Liden and Starfeldt, Phys. Rev. 97 419 (1955)
18. Bethe and Heitler, Proc. Roy. Soc. London A146 83 (1934)
19. Knipp and Uhlenbeck, Physica 3, 425 (1936)
20. Hornyak and Lauritzen, Phys. Rev. 77 160 (1950)
21. Evans The Atomic Nucleus PP 717 (1955)
22. Berger & Doggett, Bureau of Standards Journal of Research, 56, 355 - (1956)
23. Campbell & Boyle, Australian Journal of Physics, 6, 171 (1953)
24. Foote & Koch, Rev. Sci. Inst. 25, 746 (1954)
25. Bair, Kington, and Williard, Phys. Rev. 100 , 22 (1955)